Implications of the HIV-1 Rev dimer structure at 3.2 Å resolution for multimeric binding to the Rev response element

Michael A. DiMattia[a,b], Norman R. Watts[c], Stephen J. Stahl[c], Christoph Rader[d], Paul T. Wingfield[c], David I. Stuart[a], Alasdair C. Steven[b,1], and Jonathan M. Grimes[a]

[a]Division of Structural Biology, Wellcome Trust Centre for Human Genetics, Oxford University, Roosevelt Drive, Oxford, OX3 7BN, UK; [b]Laboratory of Structural Biology Research, National Institute of Arthritis and Musculoskeletal and Skin Diseases, National Institutes of Health, Bethesda, MD 20892-8025; [c]Protein Expression Laboratory, National Institute of Arthritis and Musculoskeletal and Skin Diseases, National Institutes of Health, Bethesda, MD 20892-2775; and [d]Experimental Transplantation and Immunology Branch, Center for Cancer Research, National Cancer Institute, National Institutes of Health, Bethesda, MD 20892-1203

Edited by Adriaan Bax, National Institute of Diabetes and Digestive and Kidney Diseases, Bethesda, MD, and approved February 11, 2010 (received for review December 23, 2009)

HIV-1 Rev is a small regulatory protein that mediates the nuclear export of viral mRNAs, an essential step in the HIV replication cycle. In this process Rev oligomerizes in association with a highly structured RNA motif, the Rev response element. Crystallographic studies of Rev have been hampered by the protein's tendency to aggregate, but Rev has now been found to form a stable soluble equimolar complex with a specifically engineered monoclonal Fab fragment. We have determined the structure of this complex at 3.2 Å resolution. It reveals a molecular dimer of Rev, bound on either side by a Fab, where the ordered portion of each Rev monomer (residues 9–65) contains two coplanar α-helices arranged in hairpin fashion. Subunits dimerize through overlapping of the hairpin prongs. Mating of hydrophobic patches on the outer surface of the dimer is likely to promote higher order interactions, suggesting a model for Rev oligomerization onto the viral RNA.

nuclear export | ribonucleoprotein structure | Fab cocrystallization | posttranscriptional regulation | crystal structure

The unspliced and partially spliced viral mRNAs whose nuclear export is promoted by the 13 kDa HIV-1 Rev protein (1, 2) are used both as genomic RNA for packaging into assembling virions and for translation of many of the viral proteins (3), thereby eliciting the transition from early to late phase infection (1). Rev targets viral mRNAs by recognizing a ∼350 nt, highly structured region within an *env* intron known as the Rev response element (RRE) (4). Rev then oligomerizes onto the RRE to form a ribonucleoprotein (RNP) complex of 200–300 kDa containing 8–10 Rev molecules (5, 6) that binds Crm-1 (exportin-1), GTP-bound Ran, and other host cell proteins via the Rev nuclear export sequence (NES), to promote nuclear export (7). Rev contains an arginine-rich RNA-binding motif (ARM) that specifically binds to a purine-rich bulge within stem loop IIb of the RRE (2, 8) with high affinity to nucleate assembly of the Rev–RRE complex (9, 10). Subsequently, 7–9 additional Rev molecules are recruited (4–6, 11), one at a time, in a highly cooperative process mediated primarily through Rev–Rev interactions (5, 12–14). As befits their biological importance, the interactions whereby Rev recognizes RRE-containing RNAs have been intensively studied, as has Rev's propensity to oligomerize, both in the absence of RNA and in the context of the RRE (9, 10, 15, 16).

Knowledge of Rev structure is essential to understanding its cooperative binding to the RRE and for the development of antiviral drugs that interfere with Rev's essential functions. So far, detailed structural information has been limited to an NMR structure of a 22-residue synthetic polypeptide corresponding to the ARM in complex with stem loop IIb (8). Rev's propensity to oligomerize into filaments (16) has hindered crystallization. Using a Fab engineered to inhibit Rev polymerization, we have been able to purify and crystallize a Rev–Fab complex (17). Here we report the structure determination of this complex.

Results and Discussion

The Rev–Fab crystal structure was solved at 3.2 Å resolution by molecular replacement, using model Fab structures from the PDB (*Materials and Methods*). Data collection and refinement statistics are given in Table 1 (R_{work} and $R_{free} = 0.235$ and 0.250, respectively). The *P*1 crystal's unit cell contains six Fab fragments and six Rev monomers, arranged as heterotetramers (Fig. S1), each comprising a Rev dimer flanked by two Fabs. The Fabs' variable domains provide most of the crystal contacts.

Although full-length Rev is present in the crystals (SDS–PAGE of a crystal showed unaltered Rev mobility, with contaminants at ∼5%) (Fig. S2), only residues 9 to 65—the N-terminal domain (NTD)—were found to be ordered (Fig. 1*A*). The NTD adopts a helix-loop-helix motif (herein termed a helical hairpin) (Fig. 1*B* and Fig. S3), consistent with previous proposals (16, 18–21). One prong of the hairpin consists of an α-helix (α1), residues 9 to 24, followed by the loop region from residue 25 to 33; a longer α-helix (α2), residues 34 to 65, contributes the second prong (Fig. 1*B*). The α-helices of the hairpin form a planar structure, different from a previously proposed model (19). The two faces of this helical platform are denoted A and B (Fig. 1*D*). Helix α1 and the C-terminal half of α2 are amphipathic, with hydrophobic and polar surfaces on opposing sides of the helix. The N-terminal half of α2 is the RRE-binding ARM, densely populated with Arg and Glu residues (Fig. 1*B*). Nonpolar residues cluster around the apposed surfaces of α1 and α2 to form a hydrophobic core that serves at least two purposes: (i) stabilization of the hairpin; and (ii) presentation of hydrophobic surface patches, one on each face of the hairpin (Fig. 2 *A* and *B*) that mediate interaction with other Rev monomers (see below).

The residues within the core identified by buried surface area analysis (Table S1) as major contributors to stabilizing the helical hairpin are L12, I19, L22, Y23, W45, I52, I59, L60, and Y63. Of these, four—I19, L22, I52, I59—have been proposed on other grounds to contribute to an intramolecular interface (19). Mutations at these positions reduce the affinity of Rev monomers for RRE stem-loop IIb, despite their lying outside the RNA-binding

Author contributions: N.R.W., P.T.W., D.I.S., A.C.S., and J.M.G. designed research; M.A.D. performed research; N.R.W., S.J.S., and C.R. contributed new reagents/analytic tools; M.A.D., P.T.W., D.I.S., A.C.S., and J.M.G. analyzed data; and M.A.D., P.T.W., D.I.S., A.C.S., and J.M.G. wrote the paper.

The authors declare no conflict of interest.

This article is a PNAS Direct Submission.

[1]To whom correspondence should be addressed. E-mail: stevena@mail.nih.gov.

This article contains supporting information online at www.pnas.org/cgi/content/full/0914946107/DCSupplemental.

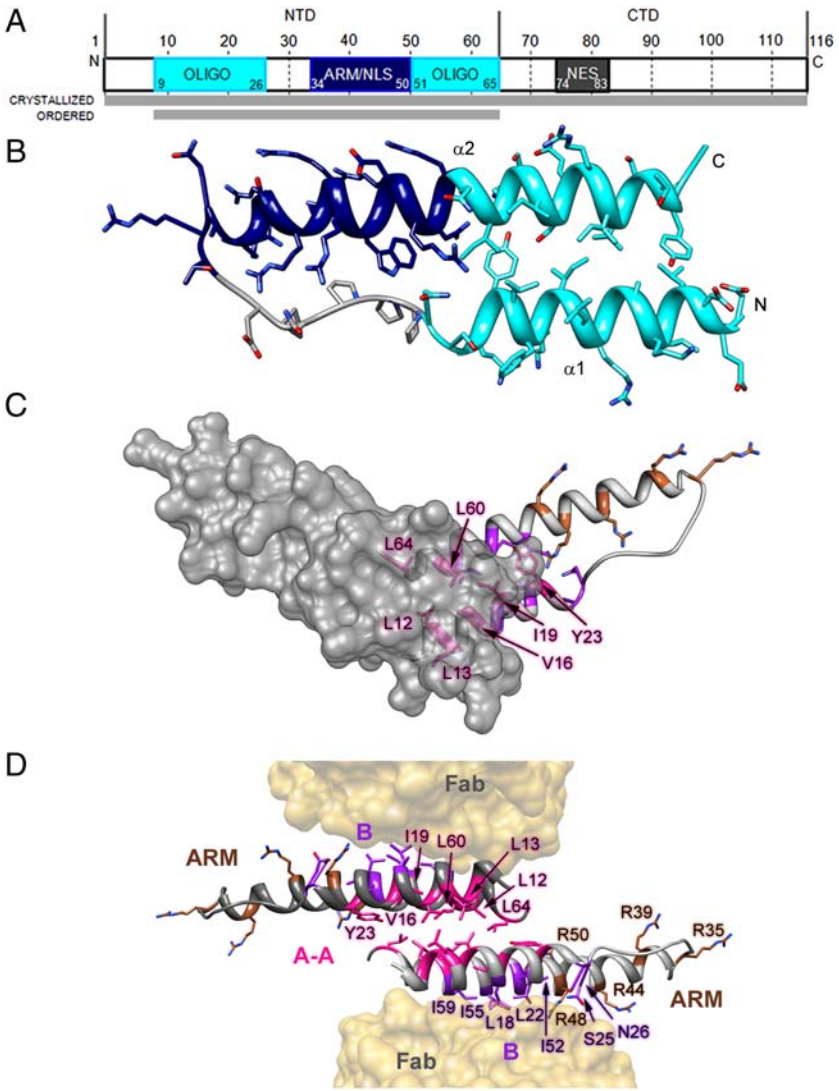

Fig. 1. Rev monomer and dimer structures. (*A*) Domain organization of Rev. Oligomerization motifs depicted in cyan, arginine-rich motif (ARM)/nuclear localization sequence (NLS) in navy blue, and nuclear export signal (NES) in dark gray. Although full-length Rev was crystallized, only the N-terminal domain was ordered. (*B*) Ribbon representation of Rev monomer (top view) showing the helix-loop-helix motif with coplanar helices. (*C*) Top down view of Rev dimer depicting residues involved in A-A interface in pink, residues implicated in B-B oligomerization and RRE binding in purple and brown, respectively; one Rev subunit is shown by isosurface rendering. (*D*) Ribbon representation of Rev dimer, depicting the A-A dimer interface and the B oligomerization faces contacting the Fabs (see Fig. 2). The oligomerization surfaces and ARM motifs are segregated, consistent with the cooperative model of Rev multimerization on the RRE (coloring as in *C*).

domain. It is likely that hydrophobic-to-hydrophilic mutations in these residues unhinge the helical hairpin and disorder the ARM, preventing the initial RRE-binding event. The interhelix loop region probably also contributes to structural integrity, due to three consecutive prolines (sequence, NPPPNPEGT) that form a rigid, concave stretch that is stabilized by the side-chain of W45. Supporting this, the electron density for this region is stronger than for the rest of the loop.

The crystal structure reveals molecular dimers of Rev flanked by Fabs (Fig. 2 *A* and *B*). The Rev dimer interface is formed by the hydrophobic patch on surface A at the pronged end of the hairpin, where the subunits overlap by two helical turns (Fig. 2*B*). The two subunits are related by an almost exact twofold axis (between 177° and 180°) and rest across each other at an angle of ~140° (Fig. 2*B*). In the dimer, identical A-surfaces mate (i.e., in a head-to-head as opposed to a head-to-tail interaction), while the B surfaces interact with Fabs (Figs. 1*D* and 2*A*). Thomas et al. originally proposed the existence of one oligomerization interface (22), but more recent reports are consistent with the two composite-face oligomerization model defined by residues upstream and downstream of the ARM (19, 23). Indeed, a Rev oligomerization model based on the analysis of assembly-defective mutants supports the idea of an alternating series of symmetrical interactions: A-A; B-B; A-A, etc. (19). The dimerization footprint (Fig. 3*C*) on surface A matches closely with the location of its hydrophobic patch (Fig. 3*A*). This is consistent with previous reports that Rev self-association is mediated predominantly by hydrophobic interactions (19). It is noteworthy that the hydrophobic patch on surface B (Fig. 3*B*) coincides with the Rev epitope for this Fab (Fig. 3*D*) (17). One can thus envision that in the absence of Fab, Rev dimers could assemble further via B-B interactions as well. The hydrophobic patches required for dimerization, and (by inference) higher order assembly, localize to the pronged end of the Rev monomer and are thus segregated from the RNA-binding ARM at the other end.

Detailed analysis of the residues involved in the A-A interface is presented in Fig. 1*C* and Table S1. As the hydrophobic residues L12, L13, V16, I19, L60, and L64 consistently bury more than

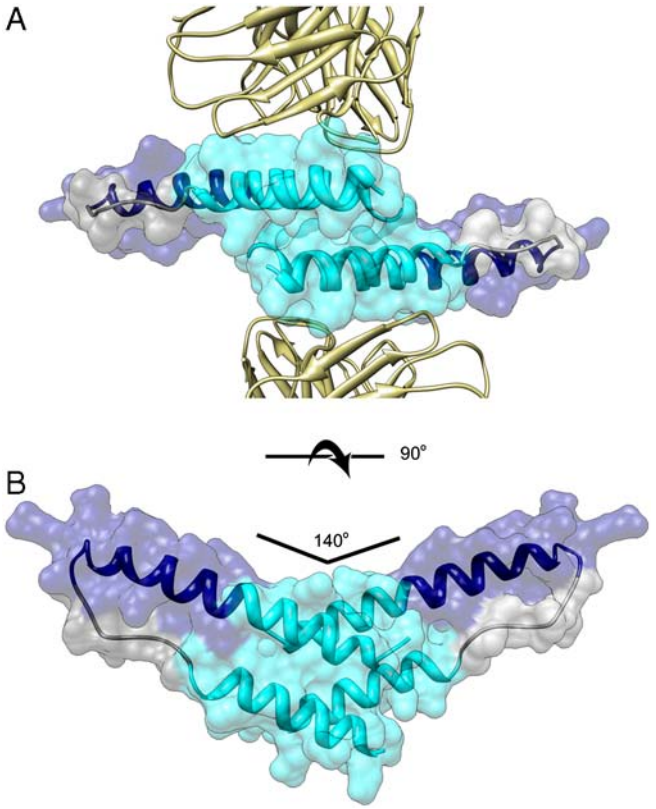

Fig. 2. Orthogonal views of the Rev crystal dimer. (*A*) Ribbon structure of the Rev dimer flanked by two Fab molecules in gold. (*B*) Top down view of Rev dimer showing the 140° interaxial angle. Coloring of Rev subunits are same as in Fig. 1 (oligomerization domains in cyan and RRE in navy blue).

50% of their surface areas at the interface, it is clear that they make key stabilizing interactions. The dimer structure is consistent with a wealth of biochemical and genetic data on the functional relevance of specific residues in Rev oligomerization. Jain and Belasco identified L12, V16, L60, and L18, L55 as key residues mediating Rev oligomerization, and these sets of residues map exactly to the A face and the B face, respectively (19). However, Edgcomb et al. further analyzed the effect of aliphatic-to-polar mutations in residues V16, L18, L55, and L60 and found that the mutants' reduced RRE-binding and nuclear export activities are more closely correlated with destabilization of Rev tertiary structure than simply the ablation of oligomerization faces A and B (23). Interestingly, they determined that of the residues investigated, polar substitutions at only residue 18 disrupt Rev oligomerization without altering Rev structure (23). While the other residues form the "core" of Rev, L18 sits at the edge of the hydrophobic cluster where it can affect oligomerization without compromising Rev structure. Additionally, the lateral position for L18 may explain its putative role in HIV-1 latency by slightly hindering Rev oligomerization, which in turn reduces Rev function, leading to less Gag expression and greater possibility for infected cells to escape anti-Gag cytotoxic T-cell responses. Mutations of the polar residues Y23, S25, and N26 disrupt oligomerization, resulting in an increased cytoplasmic concentration of Rev (2, 24, 25). Y23 makes significant contacts both within the Rev monomer and at the A-A interface, explaining the functional phenotype; S25 and N26 are on the B-surface and so support the imputed role of this surface in Rev oligomerization.

The Rev dimer structure also provides insight into Rev-RRE interactions, which we modeled by superposing the NMR structure (pdb id: 1ETF) of the stem loop IIb-ARM complex onto the Rev crystal dimer (Fig. 3*G* and *H*). The RNA helix is positioned such that there are no steric clashes with the Rev dimer and there is ample clearance for the binding of additional dimers. The two

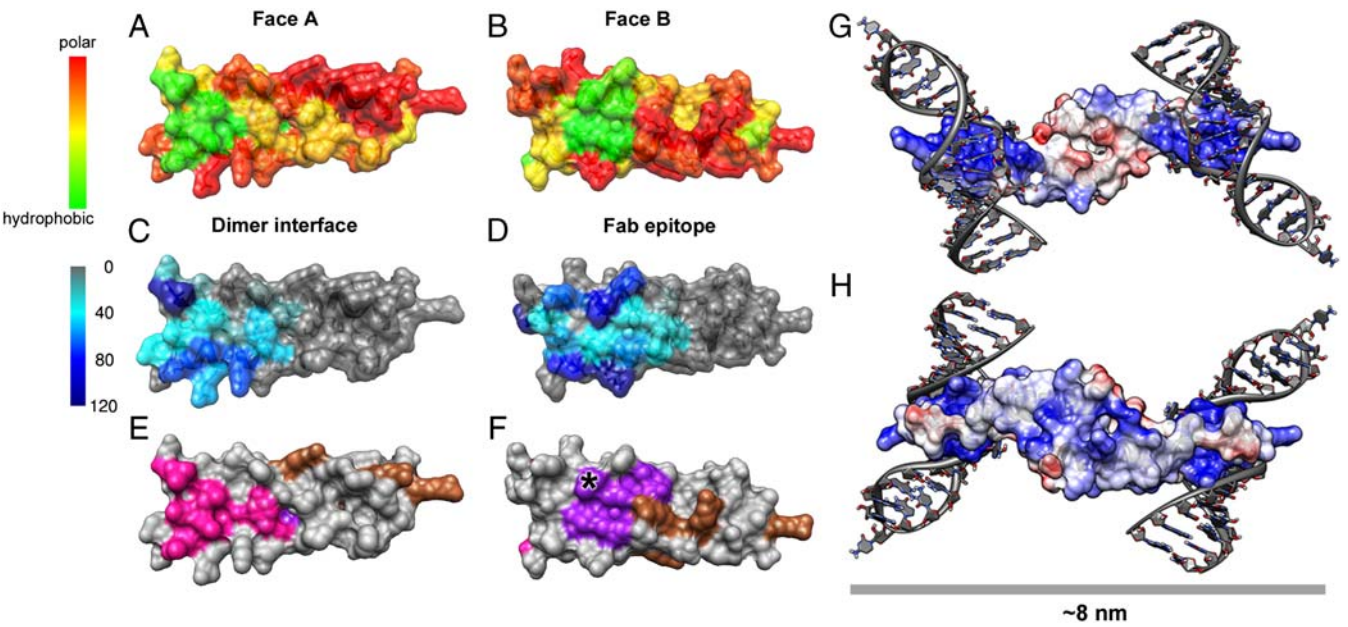

Fig. 3. Rev oligomerization faces and Rev dimer-RRE modeling. (*A*–*F*) Rev monomers are isosurface-rendered and colored according to: (*A* and *B*) surface hydrophobicity; (*C* and *D*) buried surface area at the Rev A-A dimer and Rev–Fab Face B interfaces, respectively, in Å^2; (*E* and *F*) residues shown to be involved in Rev multimerization in pink and purple for Faces A and B, respectively. Residues important for RRE interaction are depicted in brown.; L18 is marked with an asterisk to show its lateral position within the B Face. (*G* and *H*) Rev dimer in the context of Stem Loop IIB (SLIIB) high-affinity RRE-binding site. The two views are related by a 180° rotation about a horizontal axis. SLIIB RNA nucleotides from NMR structure of SLIIB bound to Rev alpha helix (res 33–55) were superposed onto the Rev dimer (rmsd of 0.8 Å over main chain atoms of residues 37–55). The width of the dimer-RNA structure above is 8 nm, consistent with the 8nm diameter of Rev-RNA filament assemblies as observed in EM (9, 10, 15, 16). Molecules are colored according to surface charge, from acidic (*Red*) to basic (*Blue*).

Table 1. Data collection and refinement statistics

	HIV-1 Rev–Fab
Data collection	
Space group	*P*1
Cell dimensions	
a, *b*, *c* (Å)	87.7, 87.7, 176.3
α, β, γ (°)	94.9, 95.5, 104.6
Resolution (Å) *	48.8–3.2 (3.3–3.2)
$R_{sym(\%)}$	11.5 (100)
$I/\sigma I$	9.9 (1.1)
Completeness (%)	99.0 (98.8)
Redundancy	3.4 (3.4)
Refinement	
Resolution (Å)	48.8–3.2
No. reflections	83,636
R_{work}/R_{free} †	23.5, 25.0
No. protein atoms	22,554
Average protein B-factor (Å^2)	144
Rms deviations	
Bond lengths (Å)	0.010
Bond angles (°)	1.3
B-factor of bonded atoms (Å^2)	18
NCS related Rev coords (Å)	0.4
NCS related Rev B-factors (Å^2)	14
NCS related Fab coords (Å)	0.2
NCS related Fab B-factors (Å^2)	33

*Highest resolution shell is shown in parentheses.

†5% of the total reflections were excluded for cross-validation. The structure was determined from data derived from a single crystal. These R-factors are derived from Buster (29) taking account of disordered unmodeled portions of the structure.

ARMs per dimer are at opposite ends of this elongated molecule, and when one subunit is modeled as RRE-bound, the other subunit clearly cannot bind to an adjacent groove of the same RNA helix. We have thus modeled two stem loops onto the dimer, the dyad axis aligning the two RREs into a track upon which additional Rev molecules might bind. In this model, stacked Rev dimers present arrays of ARMs spaced 20–25 Å apart, consistent with such an array making repetitive interactions with successive major grooves along the same side of the RNA helix. Because it has been shown that the ARM can bind RNA with different helical faces (14), Rev has some flexibility with which to bind additional RNA grooves as it multimerizes. This model is very different from an earlier one (19) in which the angle between interacting Rev monomers is far more acute. There is evidence that subsequent to the initial RNA–Rev binding event, additional Rev molecules add into the complex by binding along stem loop I (5, 12). While the structure of the RRE is largely unknown, it is plausible that stem loop I provides an opposing second RNA helix for binding on the opposite side of dimer from the initial stem loop IIb interaction.

Adjacent to the points at which the disordered residues 1–7 and 68–116, must join the ordered structure are regions of weak (~0.8σ), protein-like density without clear connectivity. One possibility is that the disordered CTD becomes partly or completely folded in the context of complex formation and/or higher order Rev multimerization, because Rev also interacts with many other cellular factors and viral proteins. Once the interfaces involved in these interactions become apparent, further insight into their functional roles should follow. In the meantime, our model of the Rev dimer reveals key features of the organization of the initial Rev-RRE complex, including segregation of the surfaces that modulate oligomerization from the RNA-binding ARM regions, thus allowing us to propose how the structural organization of Rev dimers drives the nonspecific binding of RNA.

Materials and Methods

Preparation of the Rev–Fab Complex. The design, production, purification, and biochemical characterization of this complex are described in detail in a separate paper. In brief, Rev (clone BH10) was expressed in *Escherichia coli* and purified as described (16). In labeling residues in the Rev structure and referencing mutation studies etc., we have observed the usual convention of Met being position 1; however, in the *E. coli*-produced protein, the N-terminal Met has been processed and the actual N-terminus is Ala. The urea concentration was adjusted to 1 M and a fivefold molar excess was mixed with the chimeric rabbit/human anti-Rev Fab, also in 1 M urea. The urea was needed to prevent Rev from precipitating and to maintain the solubility of the Fab. The mixture (at ~1 mg/ml protein) was dialyzed against PBS, any precipitated protein (usually excess Rev) removed by centrifugation, and then applied to a Ni-Sepharose Fast Flow column equilibrated in dialysis buffer. The Rev–Fab complex was eluted with imidazole, dialyzed against 20 mM HEPES (pH 8.0) and concentrated to 8–9 mg/mL using an Amicon Ultra-15 10K NMWCO centrifugal filter (Millipore). The His-tag at the C terminus of the C_H chain was not removed prior to crystallization.

Crystallization and Data Collection. Crystallization trials were performed at a protein concentration of 9.6 mg/mL in 20 mM HEPES pH 8.0 at 21 °C in hanging drops. Microcrystals grew in 12% PEG 6000, 100 mM diammonium phosphate (DAP), and 100 mM Tris (pH 8.5). Optimized crystals grown with 50 mM spermidine added to the drop and in 9–14% PEG 600, 100–200 mM DAP, 100 mM Tris (pH 8.5) were cryoprotected (25% v/v ethylene glycol) and flash frozen (SI Text). Diffraction data were recorded from a single crystal to a minimum Bragg spacing of 3.2 Å at the Diamond Light Source, Beamline I02, Didcot, UK. Diffraction data were integrated and scaled using HKL2000 (HKL Research, Inc.).

Structure Solution and Refinement. Initial phase information was obtained via an automated Phaser molecular replacement search using a set of published Fab structures as search models. The Fold and Function Assignment System (FFAS03) web server was utilized to identify the 10 light and heavy chain Fab structures in the PDB with the highest sequence homology to the corresponding sequences of the anti-Rev Fab (26). The correct solution was found by superimposing 18 Fab structures (*SI Text*) on both the variable and constant domains and using them as one search ensemble in Phaser (27). The space group is P1 with six Fab molecules and six Rev subunits (three dimers) in the asymmetric unit. The molecular replacement solution was rigid body-refined in Phenix with each Ig domain treated separately. Positional refinement and group B-factor refinement (one group per residue) were carried out in iteratively in both Phenix (28) and AutoBuster (29). Care was taken throughout refinement so as not to overfit the data. The Rev structure was manually built de novo by first placing two α-helices in the strong tubular density, using Coot (30). The directionality of and connectivity of the two helices were determined by placing the bulky side-chains of F17, Y21, W45, and Y63 (Fig. S3) in the N-terminal half. Final NCS-restrained (sixfold) refinement was performed in AutoBuster (27). No biochemical data on Rev was used to guide Rev building, except the primary sequence. Thus, the collected biochemical literature is in essence a check on the validity of the structure. The Molprobity server (31) and the validation tools in Coot informed the quality of the structure refinement process. Refinement statistics are given in Table 1, and final refined coordinates and structure factors have been deposited with the PDB with accession code 2X7L.

Structure Analysis. PISA Interface Web server was utilized for buried surface area and interacting residue analysis of the Rev–Fab epitope, the Rev-Rev dimer interface, and the residues contributing to structural integrity of the Rev monomer (32). The interaxial dimer angle between two Rev subunits was determined manually by calculating the dot product of the vectors parallel to α2 of each dimer subunit. Molecular graphics were produced using Chimera (33) and Pymol (DeLano Scientific LLC).

ACKNOWLEDGMENTS. We thank Drs. N. Noinaj and S. Buchanan for advice and provision of resources during the initial crystallization experiments; Drs. E. Kandiah and S. Graham for insightful discussions; and the staff at Diamond Light Source beamline I02 for support in data collection. This work was supported in part by the Intramural Research Programs of the National Institute for Arthritis and Skin Diseases and the National Cancer Institute, the National Institutes of Health (NIH) Intramural Targeted Antiviral Program, and the NIH–Oxford Scholars Program. D.I.S. is supported by the UK Medical Research Council and J.M.G. by SPINE2COMPLEXES (LSHGCT-2006-031220). The Wellcome Trust is acknowledged for providing administrative support (Grant 075491/Z/04).

1. Pollard VW, Malim MH (1998) The HIV-1 Rev protein. *Annu Rev Microbiol* 52:491–532.
2. Malim MH, Hauber J, Le SY, Maizel JV, Cullen BR (1989) The HIV-1 rev trans-activator acts through a structured target sequence to activate nuclear export of unspliced viral mRNA. *Nature* 338:254–257.
3. Tiley LS, Malim MH, Tewary HK, Stockley PG, Cullen BR (1992) Identification of a high-affinity RNA-binding site for the human immunodeficiency virus type 1 Rev protein. *Proc Natl Acad Sci USA* 89:758–762.
4. Daly TJ, Cook KS, Gray GS, Maione TE, Rusche JR (1989) Specific binding of HIV-1 recombinant Rev protein to the Rev-responsive element in vitro. *Nature* 342:816–819.
5. Mann DA, et al. (1994) A molecular rheostat. Co-operative Rev binding to stem I of the Rev-response element modulates human immunodeficiency virus type-1 late gene expression. *J Mol Biol* 241:193–207.
6. Daly TJ, et al. (1993) Biochemical characterization of binding of multiple HIV-1 Rev monomeric proteins to the Rev-responsive element. *Biochemistry* 32:10497–10505.
7. Suhasini M, Reddy TR (2009) Cellular proteins and HIV-1 Rev function. *Curr HIV Res* 7:91–100.
8. Battiste JL, et al. (1996) Alpha helix-RNA major groove recognition in an HIV-1 Rev peptide-RRE RNA complex. *Science* 273:1547–1551.
9. Bogerd H, Greene WC (1993) Dominant negative mutants of human T-cell leukemia virus type I Rex and human immunodeficiency virus type 1 Rev fail to multimerize in vivo. *J Virol* 67:2496–2502.
10. Malim MH, Bohnlein S, Hauber J, Cullen BR (1989) Functional dissection of the HIV-1 Rev trans-activator—derivation of a trans-dominant repressor of Rev function. *Cell* 58:205–214.
11. Malim MH, Cullen BR (1991) HIV-1 structural gene expression requires the binding of multiple Rev monomers to the viral RRE: Implications for HIV-1 latency. *Cell* 65:241–248.
12. Pond SJ, Ridgeway WK, Robertson R, Wang J, Millar DP (2009) HIV-1 Rev protein assembles on viral RNA one molecule at a time. *Proc Natl Acad Sci USA* 106:1404–1408.
13. Cook KS, et al. (1991) Characterization of HIV-1 Rev protein: Binding stoichiometry and minimal RNA substrate. *Nucleic Acids Res* 19:1577–1583.
14. Daugherty MD, D'Orso I, Frankel AD (2008) A solution to limited genomic capacity: Using adaptable binding surfaces to assemble the functional HIV Rev oligomer on RNA. *Mol Cell* 31:824–834.
15. Watts NR, et al. (1998) Three-dimensional structure of HIV-1 Rev protein filaments. *J Struct Biol* 121:41–52.
16. Wingfield PT, et al. (1991) HIV-1 Rev expressed in recombinant *Escherichia coli*: Purification, polymerization, and conformational properties. *Biochemistry* 30:7527–7534.
17. Stahl SJ, et al. (2010) Generation and characterization of a chimeric rabbit/human Fab for co-crystallization of HIV-1 Rev. *J Mol Biol*, in press.
18. Blanco FJ, Hess S, Pannell LK, Rizzo NW, Tycko R (2001) Solid-state NMR data support a helix-loop-helix structural model for the N-terminal half of HIV-1 Rev in fibrillar form. *J Mol Biol* 313:845–859.
19. Jain C, Belasco JG (2001) Structural model for the cooperative assembly of HIV-1 Rev multimers on the RRE as deduced from analysis of assembly-defective mutants. *Mol Cell* 7:603–614.
20. Auer M, et al. (1994) Helix-loop-helix motif in HIV-1 Rev. *Biochemistry* 33:2988–2996.
21. Havlin RH, Blanco FJ, Tycko R (2007) Constraints on protein structure in HIV-1 Rev and Rev-RNA supramolecular assemblies from two-dimensional solid state nuclear magnetic resonance. *Biochemistry* 46:3586–3593.
22. Thomas SL, et al. (1998) Functional analysis of the human immunodeficiency virus type 1 Rev protein oligomerization interface. *J Virol* 72:2935–2944.
23. Edgcomb SP, et al. (2008) Protein structure and oligomerization are important for the formation of export-competent HIV-1 Rev-RRE complexes. *Protein Sci* 17:420–430.
24. Szilvay AM, Brokstad KA, Boe SO, Haukenes G, Kalland KH (1997) Oligomerization of HIV-1 Rev mutants in the cytoplasm and during nuclear import. *Virology* 235:73–81.
25. Trikha R, Brighty DW (2005) Phenotypic analysis of human immunodeficiency virus type 1 Rev trimerization-interface mutants in human cells. *J Gen Virol* 86:1509–1513.
26. Jaroszewski L, Rychlewski L, Li Z, Li W, Godzik A (2005) FFAS03: A server for profile–profile sequence alignments. *Nucleic Acids Res* 33:W284–288.
27. McCoy AJ, et al. (2007) Phaser crystallographic software. *J Appl Crystallogr* 40:658–674.
28. Adams PD, et al. (2010) PHENIX: A comprehensive Python-based system for macromolecular structure solution. *Acta Crystallogr* D66:213–221.
29. Blanc E, et al. (2004) Refinement of severely incomplete structures with maximum likelihood in BUSTER-TNT. *Acta Crystallogr D* 60(Pt 12 Pt 1):2210–2221.
30. Emsley P, Cowtan K (2004) Coot: Model-building tools for molecular graphics. *Acta Crystallogr D* 60:2126–2132.
31. Davis IW, et al. (2007) MolProbity: All-atom contacts and structure validation for proteins and nucleic acids. *Nucleic Acids Res* 35(Web Server issue):W375–383.
32. Krissinel E, Henrick K (2007) Inference of macromolecular assemblies from crystalline state. *J Mol Biol* 372:774–797.
33. Pettersen EF, et al. (2004) UCSF Chimera—A visualization system for exploratory research and analysis. *J Comput Chem* 25:1605–1612.